ICMERE2013-PI-026

ELASTIC, ELECTRONIC AND OPTICAL PROPETIES OF TWO NEW PHASES OF SnH$_4$: FIRST PRINCIPLES STUDY

M. M. Ali[1] and A.K.M.A. Islam[2]

[1,2]Department of Electrical and Electronic Engineering, International Islamic University Chittagong (IIUC), Bangladesh.

[1]mozaharrubd@gmail.com, [2]azi46@ru.ac.bd

Abstract- *The elastic, electronic and optical properties of two newly predicted (Cmcm, P2$_1$/m) phases of SnH$_4$ using first principle calculations is reported here. It is found for the pressure less than 80 GPa the orthorhombic (Cmcm) and the monoclinic (P2$_1$/m) structures are to be energetically more favorable than the Ama$_2$ and P6$_3$/mmc structures. The elastic constants (C$_{ij}$), the electronic band structures, the density of states (DOS) and the phonon frequencies are calculated for the first time. The band structures show metallic character with large dispersion bands crossing the Fermi level (E$_F$) for both the phases. The presence of flat bands near the Fermi level provides favorable conditions for enhancing electron pairing, which implies superconducting behavior. The optical properties (dielectric function, refractive index, absorption, loss function and reflectivity) of these two phases for the first time have been discussed.*

Keywords: Phase stability, Elastic properties, Electronic properties, Optical properties

1. INTRODUCTION

It was first proposed by Wigner and Huntingdon [1] that hydrogen would become metallic under sufficiently strong compression, because hydrogen is the lightest and relatively simplest of the elements and can form a diatomic molecular gas at ambient conditions. Metallic hydrogen is also predicted to be superconducting with a high transition temperature [2, 3]. The heavy hydrides of group IVA elements [C, Si, Ge, and Sn] would become metallic and superconducting state at lower pressures [4] because the hydrogen has already been chemically compressed in these hydride compounds. The previous theoretical studies predict that stannane (SnH$_4$) [5-6], silane (SiH$_4$) [7–11], germane (GeH$_4$) [12-14], and alane (AlH$_3$) [15] metallize and superconduct at much lower and accessible pressures. It was predicted by Zhang [14] that GeH$_4$ becomes a high-temperature superconductor with a T_c of 40 K at 20 GPa. The superconducting temperature (T_c) of SnH$_4$ can be higher and may reach up to 80 K at 120 GPa was studied by Tse *et al* [5]. They found that the high-pressure phase of SnH$_4$ has P6/*mmm* symmetry with a layered structure intercalated by molecular H$_2$ units. Two unique high-pressure metallic phases of SnH$_4$ having space groups Ama$_2$ and P6$_3$/*mmc* was proposed by Gao *et al* [6]. The T_c of these two phases was predicted to be 15-22 K and 52-62 K, at 120 and 200 GPa respectively. They further had proposed two unique new phases (Cmcm, P2$_1$/m) only, but no detailed study had been attempted except enthalpy calculation. They showed that Ama$_2$ and P6$_3$/*mmc* phases are unstable below 96 and 158 GPa for elemental decomposition but did not mention about stability of Cmcm and P2$_1$/m

phases. The heavier group IV elements such as SnH$_4$ offer some potential advantages over SiH$_4$. To get high frequency conversion efficiency, the stable SnH$_4$ gas at ambient condition was used as fuel [16]. The heavier Sn atom yields lower energy vibrations that helps to mediate electron-phonon coupling. Due to weaker Sn-H bond enthalpy, the Sn-H bond dissociates easily at lower pressure. Our calculation shows these two phases are more energetically favorable at lower pressure. It is our desire to get stable state of these phases at lower and accessible pressures. Thus it is of interest to study in detail all the relevant properties of these phases. In this present work, the structural phase stability, elastic, electronic and optical properties of these two phases are investigated and among them elastic and optical properties have been studied for the first time.

2. COMPUTATIONAL METHODS

Our calculations were performed using the *ab initio* plane-wave pseudopotential approach within the framework of the density-functional theory implemented in the CASTEP software [17]. The ultrasoft pseudopotentials were used in the calculations, and the plane-wave cutoff energy was 400 eV for both the structures. The exchange-correlation terms were considered by the Perdew-Berke-Ernzerhof form of the generalized gradient approximation [18]. The k-points samplings were 5×8×7 and 9×3×8 in the Brillouin zone for the $P2_1/m$ and Cmcm phases respectively, according to the Monkhorst-Pack scheme. All the structures were relaxed by the BFGS methods [19]. The elastic constants C_{ij}, bulk modulus B and electronic properties were

directly calculated by the CASTEP code.

3. RESULTS AND DISCUSSION

3.1 Structural Stability

In previous study [6], it was shown that the Ama_2 and $P6_3/m$ phases are energetically much more favorable than the $P6/mmm$ and $Cccm$ structures. Whereas, in our study the $Cmcm$ and $P2_1/m$ structures are energetically more favorable for the pressure less than 80 GPa than the Ama_2 and $P6_3/mmc$ structures as shown in the figure 1 (c). In $P2_1/m$ phase Sn atoms form a simple monoclinic structure with semi molecular H_2 units shown in figure 1 (b). The Sn atom occupies the crystallographic $2e$ sites (0.64826, 0.25, 0.74596) and the H atoms are on the $2e$ sites (0.92488, 0.25, 0.32702), (0.08651, 0.25, 0.38317), (0.02506, 0.25, 0.89266), and (0.18168, 0.25, 0.82398) respectively. The nearest H-H bond length, 0.785 Å at 70 GPa, is short enough to be considered as covalent bonding but significantly longer than the 0.74 Å in the free H_2 molecule. This indicates the striking feature of this structure. In orthorhombic $Cmcm$ phase as shown in the figure 1 (a), adjacent Sn layers are bridged by a pair of H atoms with a Sn-H bond length from 2.063 Å to 1.749 Å at 20 to 120 GPa. This indicates the contraction of bond lengths with pressure. In this structure the atomic positions of Sn at $4c$ (0, 0.29142, 0.25) and H at $4c$ (0, 0.50191, 0.75), (0, 0.42112, 0.75) and $8f$ (0, 0.96117, 0.49332).
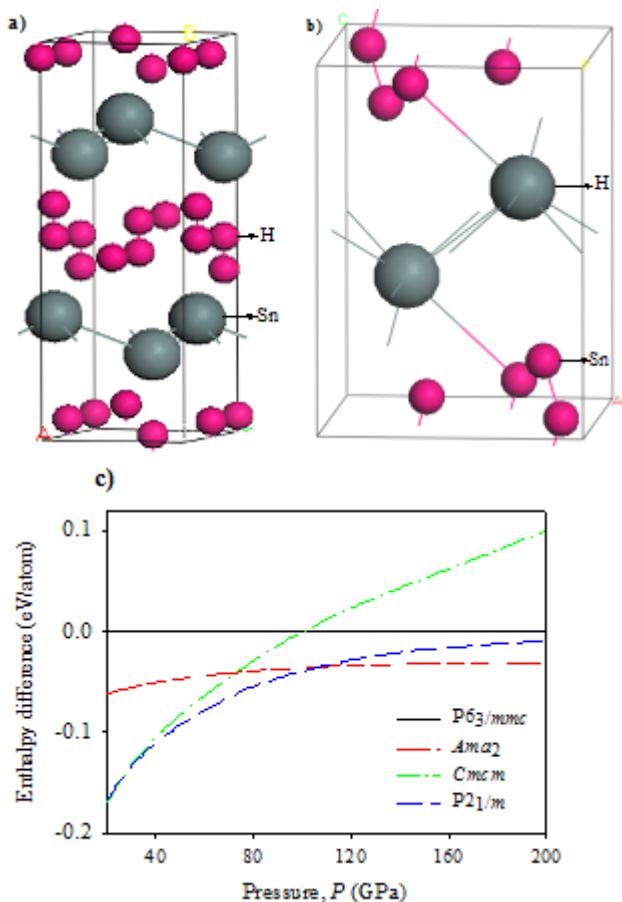
Fig.1: Structure of (a) $Cmcm$, (b) $P2_1/m$ phases at 35 and 70 GPa and (c) Enthalpy curve as a function of pressure

Table 1: The optimized equilibrium lattice parameters (in Å), cell volume V (in Å^3), total enthalpy E (in eV) and bulk modulus B (in GPa) of $Cmcm$ and $P2_1/m$.

Parameters	Structure	
	$Cmcm$ at 33 GPa	$P2_1/m$ at 70 GPa
a (Å)	3.3387	4.9315
b (Å)	9.8249	3.1644
c (Å)	4.0790	3.4914
V (Å^3/f.u)	33.45	27.24
E (eV/f.u)	-149.55	-142.68
B (GPa)	145	254

3.2 Elastic Properties

Elastic constants provide important information concerning the strength of materials, and often act as stability criteria or order parameters to study the problem of structural transformations. We calculated here the nine elastic stiffness constants (C_{ij}) for an orthorhombic ($Cmcm$ phase) system at 33 GPa as follows as; C_{11}=203, C_{22}=260, C_{33}=226, C_{44}=50, C_{55}=113, C_{66}=19, C_{12}=83, C_{13}=135, C_{23}-87 and the thirteen elastic constants for a monoclinic ($P2_1/m$ phase) system at 70 GPa as C_{11}=490, C_{22}=486, C_{33}=367, C_{44}=102, C_{55}=62, C_{66}=99, C_{12}=163, C_{13}=155, C_{15}=-22, C_{23}=184, C_{25}=34, C_{35}=-32 and C_{46}=-2. The eigenvalues of these elastic constants of the two structures fulfill the stability criteria [20] and indicate that these phases are mechanically stable. The theoretical polycrystalline elastic moduli for $Cmcm$ and $P2_1/m$ can be calculated from the set of independent elastic constants. Hill [21] proved that the upper and lower limits of the true polycrystalline constants may be represented Voigt and Reuss equations. He showed that the polycrystalline moduli are the arithmetic mean values of the moduli in the Voigt (B_V, G_V) and Reuss (B_R, G_R) approximation, and are thus given by $B_H \equiv B = \frac{1}{2}(B_R + B_V)$ and $G_H \equiv G = \frac{1}{2}(G_R + G_V)$. The Young's modulus Y and Poisson's ratio ν are then computed from these values using the relationship: $Y = 9BG/(3B+G)$, $\nu = (3B-Y)/6B$. From the calculated values of the moduli it is easy to evaluate the compressibility (β), Young's moduly (Y), and the Poisson's ratio (v) (see Table 2). The minimum value of the Poisson Ratio (v) for covalent materials is 0.1 ($v = 0.1$), increase for ionic systems [22]. In our case, the values of v for $Cmcm$ and $P2_1/m$ are 0.338 and 0.330, which indicate of sizable ionic contribution in intra-atomic bonding. According to Pugh's criteria [23], a material should behave in a ductile manner if $G/B < 0.5$, otherwise it should be brittle. Here $G/B = 0.362$ & 0.385 for $Cmcm$ and $P2_1/m$, which are indicative of ductile metallic manner.

Table 2: The values of moduli of *Cmcm* and *P2₁/m*.

Parameters	Structure	
	Cmcm	*P2₁/m*
Compressibility, β (GPa^{-1})	0.00689	0.003876
Shear moduli, G (GPa)	52.5	99.5
Young's moduli, Y (GPa)	140.5	264.5
Poisson ratio	0.338	0.330

3.3 Electronic Properties

The calculated electronic band structures and atom projected DOS for the *Cmcm* structure at 35 GPa (upper) and *P2₁/m* structure at 70 GPa (bottom) are demonstrated in the figure. 2. The band structures reveal metallic character with large dispersion bands crossing the Fermi level (E_F) for both the phases. We observed that the valence bandwidths are very broad and show strong hybridization between the Sn and H orbital. The DOS shows significantly overlap between the orbitals of the Sn and H atoms, which is in agreement with previous theoretical prediction [4]. The DOS at the Fermi level N(E_F) for *Cmcm* at 33 GPa and *P2₁/m* at 70 GPa attains the values of 1.37×10^{-2} and 1.76×10^{-2} states/eV/ Å^3, exhibiting their good metallic property. Dominant contributions to the DOS near the Fermi level come from Sn-*p* electrons. While Sn-*s* and H-*s* have minor contributions to the DOS at the Fermi level. The *P2₁/m* structure has larger electronic density of states than that of the *Cmcm* structure. This larger DOS contributes to a higher T_c. From the figure 2 (bottom), we have found the flat bands in the vicinity of E_F close to the Γ and D points. The occurrence of flat and step bands near Fermi level has been suggested as favorable conditions for enhancing electron pairing, which is essential to superconducting behavior [24].
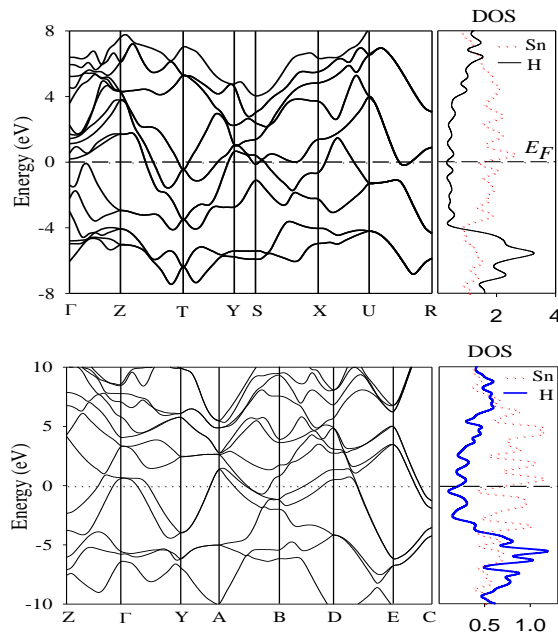

Fig. 2. Electronic band structure and atom projected DOS of *Cmcm* (upper) and *P2₁/m* (bottom).

3.4 Optical Properties

The optical properties are derived from the knowledge of the complex dielectric function $\varepsilon(\omega) = \varepsilon_1(\omega) + i\varepsilon_2(\omega)$. The imaginary part $\varepsilon_2(\omega)$ is obtained from the momentum matrix elements between the occupied and unoccupied wave functions within the selection rules, whereas the real part $\varepsilon_1(\omega)$ of dielectric function can be derived through Kramers–Kronig relations. Optical constants such as the refractive index $n(\omega)$, extinction coefficient $k(\omega)$, conductivity, optical reflectivity $R(\omega)$, absorption coefficient $\alpha(\omega)$, and energy-loss spectrum $L(\omega)$ may be computed from the values of $\varepsilon(\omega)$ using the expressions given in ref. [25].
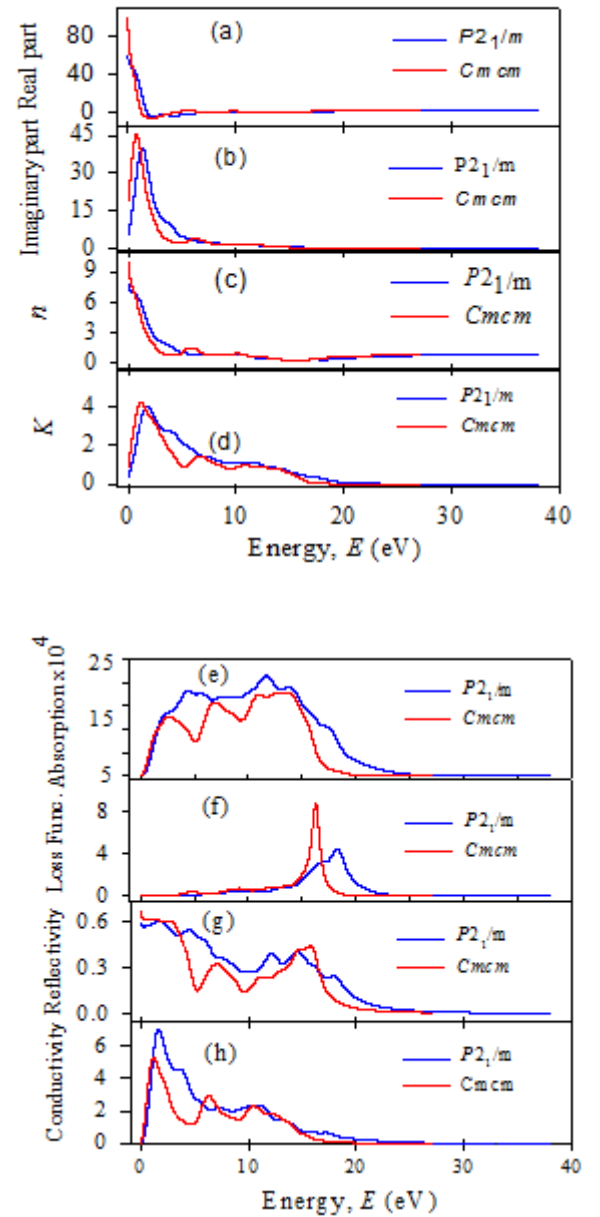

Fig.3. Energy dependent (a) real part of dielectric function, (b) imaginary part of dielectric function, (c) refractive index, (d) extinction coefficient, (e) absorption, (f) Loss function, (g) reflectivity, and (h) real part of

conductivity of $P2_1/m$ at 70 GPa and *Cmcm* at 33 GPa.

The calculated optical properties of $P2_1/m$ at 70 GPa and *Cmcm* at 33 GPa are presented in the figure.3, for the energy range up to 40 eV. The figure 3(a) and figure 3(b) show the real and imaginary parts of the dielectric function of these two phases. It is obvious from the electronic structures study that these two phases are metallic. Therefore it is required to include the effect of metallicity via an empirical Drude term to the dielectric function [25-27]. The plasma frequency 3 eV and damping (relaxation energy) 0.05 eV have been used in the Drude term. The calculated both imaginary parts, $\varepsilon_2(\omega)$ exhibit one peak located at 1.26 eV for $P2_1/m$ and 0.88 eV for *Cmcm* respectively. The origin of the peaks is attributed to the interband transition from occupied hybridized states to hybridized unoccupied states. The real parts, $\varepsilon_1(\omega)$ show that the main peaks with a magnitude of 98 and 60 are located at about 0.15 eV. The real part ε_1 goes through zero from below and the imaginary part ε_2 approaches zero from above at about 7.04 eV. The refractive index n (ω), and extinction coefficient k (ω), are illustrated in the figure 3 (c) and figure 3(d). The static refractive indexes, n (0) of these two phases are found to have the values 7.6 and 10.15 respectively. Since the materials have no band gap as evident from band structures, the photoconductivity starts with zero photon energy for each of the phases as shown in the figure 3 (h). These spectra have several maxima and minima within the energy range studied. The photo conductivities and hence electrical conductivities of materials increase as a result of absorbing photons [28].

The electron energy loss function $L(\omega)$ is depicted in the figure 3 (f). $L(\omega)$ is an important factor describing the energy loss of a fast electron traversing in a material. The peaks in $L(\omega)$ spectra represent the characteristic associated with the plasma resonance and the corresponding frequency is the so called plasma frequency ω_P [27]. The peaks of $L(\omega)$ correspond to the trailing edges in the reflection spectra. The peak of $L(\omega)$ is at about 16.3 eV and 18.2 that corresponds to plasma frequency of these phases. The calculated optical reflectivity $R(\omega)$ is displayed in the figure 3 (g). The maximum reflectivity value of about 70% to 83% occurs between the energy range 0 to 3 eV which is in the below ultraviolet region. These two phases of SnH_4 can therefore serve as possible shields for below ultraviolet radiation.

4. CONCLUSION

The structural phase stability, elastic, electronic and optical properties of two newly predicted (*Cmcm*, $P2_1/m$) phases of SnH_4 is studied theoretically. The calculated lattice parameters of these phases are in good agreement with the experimental finding. The independent elastic constants, bulk modulus, shear modulus; Young's modulus, Poisson's ratio, dielectric function refractive index, absorption, loss function, and reflectivity are calculated for the first time. These two phases are found to energetically more favorable than others.

The calculated band structure and DOS show that these two phases of SnH_4 are metallic and at the Fermi level the main contribution comes from the Sn atoms. From the analysis of optical function for polarization vector along [100] direction, it is found that the reflectivity is high in the below ultraviolet region which predicts that these two phases of SnH_4 can be used as possible shielding material for below ultraviolet radiation.

5. REFERENCES

[1] Wigner E, Huntington HB On the possibility of a metallic modification of hydrogen. J Chem Phys 3, 764–770 (1935).

[2] Ashcroft NW Metallic hydrogen: A high-temperature superconductor. Phys Rev Lett 21, 748–1749 (1968).

[3] Richardson CF, Ashcroft NW High temperature superconductivity in metallic hydrogen: Electron-electron enhancements. Phys Rev Lett 78, 118–121 (1997).

[4] Ashcroft NW Hydrogen dominant metallic alloys: High temperature superconductors. Phys Rev Lett 92, 187002 (2004).

[5] J. S. Tse, Y. Yao, and K. Tanaka, Phys. Rev. Lett. 98, 117004 (2007).

[6] Gao *et. al* High-pressure crystal structures and superconductivity of Stannane (SnH_4) PNAS January 26, vol. 107 no. 4 1317-1320 (2010).

[7] Feng J, Grochala W, Jaroń T, Hoffmann R, Bergara A, Ashcroft NW Structures and potential superconductivity in SiH4 at high pressure: En route to "metallic hydrogen.". Phys Rev Lett 96, 017006 (2006).

[8] Yao Y, Tse JS, Ma Y, Tanaka K Superconductivity in high-pressure SiH4. Europhys Lett 78, 37003 (2007).

[9] Pickard CJ, Needs RJ High-pressure phases of silane. Phys Rev Lett 97, 045504 (2006).

[10] Xiao-Jia Chen *et al* Phys.Rev.Lett. 101, 077002 (2008).

[11] Miguel Martinez-Canales*, et. al* Phys.Rev.Lett. 102, 087005 (2009).

[12] M. Martinez-Canales, *et. al* Journal of Physics and Chemistry of Solids, 67 2095–2099 (2006)

[13] Guoying Gao, et. al, Phys.Rev.Lett. 101, 107002 (2008).

[14] Chao Zhang, et. al, Superconductivity in Hydrogen-rich Material, GeH_4, J Supercond Nov Magn 23, 717–719, (2010)

[15] A. K. M. A. Islam, M. M. Ali, M. L. Ali, Physica C 470 403-406 (2010).

[16] Development of Sn- fueled high- power DPP EUV source for enabling HVM, SPIE, International EUVL Symposium (2007).

[17] S. J. Clark, M. D. Segall, C. J. Pickard, P. J. Hasnip, M. J. Probert, K. Refson, and M. C. Payne, Zeitschrift fuer Kristallographie 220, 567 (2005).

[18] J. P. Perdew, K. Burke, and M. Ernzerhof, Phys. Rev. Lett. 77, 3865 (1996).

[19] T. H. Fischer and J. Almlof: J. Phys. Chem. 96, 9768 (1992).

[20] Xiaoli Wang et al, J. Chem. Phys. 132, 024502 (2010).

[21] R. Hill, Proc. Phys. Soc. London A 65, 349 (1952).

[22] J. Haines, J. M. Leger, and G. Bocquillon, Ann. Rev. Mater. Res. 31, 1 (2001).

[23] S.F. Pugh, Phil. Mag. 45, 823 (1954).

[24] A. Simon, Angew. Chem., Int. Ed. Engl. 36, 1788 (1997).

[25] S. Li, R. Ahuja, M.W. Barsoum, P. Jena, B. Johansson, Appl. Phys. Lett. 92, 221907 (2008).

[26] R. Saniz, L. Ye, T. Shishidou, A.J. Freeman, Phys. Rev. B 74, 014209 (2006).

[27] M. Fox, Optical Properties of Solids, Academic Press, New York, 972.

[28] J. Sun, X.F. Zhou, Y.X. Fan, J. Chen, H.T. Wang, Phys. Rev. B 73 045108–045110 (2006).